


ORIGINAL ARTICLE

Open Access



# Mechanical properties of laminated bamboo lumber N-finity according to ISO 23478-2022

Layth S. Al-Rukaibawi<sup>1\*</sup> , Mansour Kachichian<sup>1</sup> and György Károlyi<sup>2\*</sup>

## Abstract

This research used the new ISO 23478-2022 standard as a reference for the calculation of mechanical properties of N-finity, and to understand the failure modes in compression. Previous studies have investigated the mechanical properties of laminated bamboo lumber (LBL), however no study has evaluated the mechanical properties of LBL according to the recently published ISO 23478-2022. The compression testing programme in parallel and perpendicular-to-grain directions were conducted. The measured elastic stiffness properties and compressive strengths show anisotropy with higher compressive strength and stiffness parallel-to-grain direction as compared to those at the transversal directions. The observed failure modes at the parallel-to-grain direction exhibited a mixed mode failure, whereas perpendicular-to-grain directions exhibited failure with longitudinal splitting with crack propagation rupture. This finding can be quantified using Hills failure criterion principle to define the failure criterion and to estimate the Hill's yield failure ratios.

**Keywords** Moso bamboo, Natural composite, Compression testing, Failure mechanisms, N-finity, ISO 23478

## Introduction

Engineered bamboo products (EBPs) made of *Phyllostachys pubescens* referred herein as 'Moso bamboo', have been researched extensively. A commercially available product of EBPs is laminated bamboo lumber named "N-Finity". This structural product is manufactured by Moso International BV in the Netherlands, and it is considered as a natural composite material with low-carbon footprint [1]. The typical manufacturing process starts with a standardised cutting of bamboo strips from the middle part of a ring-like culm wall after the removal of the skin at the outer part and the pith ring at the inner

part. The resulting product is a thick strip with cross-sectional dimensions of about 20 mm width and 6 mm thickness, see Fig. 1d. Then, the N-finity is manufactured by gluing strips utilising Phenol formaldehyde resins PF of good performance characteristics to provide an engineered composite beam, which is available with two different laminate orientations: Flatwise-section and Edgewise-section, see Fig. 1e.

Until now, many studies have been conducted on the mechanical properties of EBPs [2–6]. However, Laminated bamboo lumber (LBL) are increasingly recognised in structural applications and in building full-scale constructions. A bamboo villa was built in 2008 by Nanjing Forestry University, and a bamboo house was built by Hunan University, each of which were two-story office buildings [7, 8]. These structural buildings are formed from structural components such as beams, columns, walls, and beam-to-column connections. Several experimental investigations have determined the overall stiffness properties of LBL in compression and shear parallel and perpendicular-to-grain directions, see Table 1. The cited literature in this table concluded the importance

\*Correspondence:

Layth S. Al-Rukaibawi  
syyd.salman.al-rukaibawi@emk.bme.hu  
György Károlyi  
karolyi@reak.bme.hu

<sup>1</sup> Department of Structural Engineering, Budapest University of Technology and Economics, Műegyetem Rkp. 3, 1111 Budapest, Hungary

<sup>2</sup> Institute of Nuclear Techniques, Budapest University of Technology and Economics, Műegyetem Rkp. 3, 1111 Budapest, Hungary

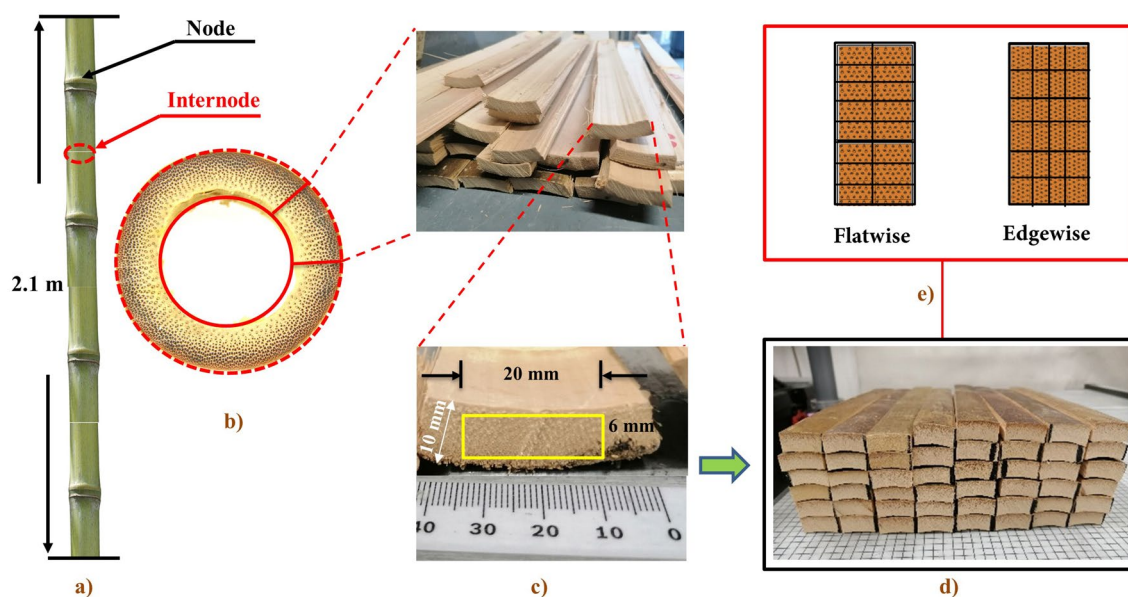


**Fig. 1** Processing overview of bamboo strips with (a) bottom part of culm, (b) bamboo cross-section wall, (c) strips cutting, (d) short bamboo strips and (e) laminate orientation: flatwise-section and edgewise-section

of LBL as a constructional material. The reported axial elastic modulus in compression parallel and perpendicular-to-grain directions were found to be about 8.7 GPa, and 1.7 GPa on average, respectively. The shear modulus was 0.5–1.4 GPa and 0.4–1.3 GPa for parallel and perpendicular-to-grain directions, respectively, whereas the compression strength parallel and perpendicular-to-grain directions were found to be within the range of 34–84 MPa, and 18–36 MPa, respectively. To conclude, these investigations were mainly conducted utilising several standards which are designed specifically for timber and polymeric composite materials rather than bamboo-based materials. In addition, the focus of the cited literature was on small clear specimens to obtain the overall stiffness properties of LBL.

However, to the authors' best knowledge, no study has evaluated the mechanical properties of LBL utilising the recently published ISO 23478-2022 [19] standard for testing structural specimens of EPBs including LBL. Therefore, the ISO 23478-2022 standard was used as a reference for the test method and the calculation of mechanical properties of a commercial type of LBL named "N-finity" in compression parallel-to-grain (axial direction), perpendicular-to-grain (tangential direction) and perpendicular-to-grain (radial direction). This is attained by experimentally testing engineered bamboo with small clear specimens at three orthogonal directions. Physical uniaxial testing in compression was conducted at the Department of Structural Engineering of the Budapest University of Technology and Economics.

The paper is divided into the following sections. Experimental programme provides a detailed description of the experimental programme including the materials used and the steps for preparing the compression specimens parallel and perpendicular-to-grain directions. In addition, the procedure and measurement of oven-dry density and moisture content of the specimens are briefly described. The results and discussion reports the results of oven-dry density, moisture content and experimental uniaxial compression test specimens, and the measured elastic modulus and compressive strengths, all of which are compared with reported previous experimental results. Also, in the Results and discussion, the failure modes of N-finity Moso bamboo are presented. Hill's failure criterion and mechanical properties of N-finity Moso bamboo gives a brief overview of the estimated mechanical properties of N-finity Moso bamboo using Hill's failure criterion. Finally, Conclusion and future work describe the main conclusions and areas for further research.

## Experimental programme

### Materials and compression specimen preparation

The N-finity beam is an LBL product commercially available in Hungary from the company Introwood who imported it from the Netherlands. This product was manufactured from the middle layers of four-year-old moso bamboo. The engineered beams have a dimension of 2000 mm length, 36 mm width and 80 mm height or depth. The laminate orientation of N-finity beam is



**Table 1** (continued)

Refs.	Standard testing methods	Density ( $\rho$ ) kg/m <sup>3</sup>	Lamina direction	MC%	Compression properties			Poisson's ratio			Shear properties		
					Modulus (GPa)	Strength (MPa)	$f_{11}$ $f_{22}$ $f_{33}$	$\nu_{12}$	$\nu_{13}$	$\nu_{23}$	Modulus (GPa)	Strength (MPa)	$f_{12}$ $f_{13}$ $f_{23}$
This study	ISO 23478–2022	625	Flatwise	7.2	8.75 2.19 1.11	68.60 15.41 13.16	0.24	0.35	0.52	1.97 1.38 0.51	16.03 6.59 4.43		

Flatwise, see Fig. 2a. The compression specimens, cut from the engineered beams, formed three groups: group a: parallel-to-grain, longitudinal (L) or  $x$  axis, group b: perpendicular-to-grain, tangential (T) or  $y$  axis, and group c: along the thickness, radial (R) or  $z$  axis. To prepare specimens of group a, the short rectangular beam of depth 80 mm was cut longitudinally into two-halves and machined to the required size (see Table 2) using an electric sawing band. Specimens of group b were prepared by cutting longitudinally the short rectangular beam of depth 80 mm into two-halves which are glued to each other sideway (c.f. Figure 2b) s applying an epoxy adhesive named Araldite 2011, a two-component glue supplied by the Hungarian company Neosil Kft. Specimens of group c were prepared after cutting the N-finity beam into small cuboids of length 36 mm. As a result, 16 specimens of each group were prepared, resulting in a total of 48 cuboid samples prepared for compression testing in all three directions (longitudinal, tangential, radial). Five specimens for each group were equipped with 4 strain gauges as shown in Fig. 2b to measure the strains and to obtain the Poisson's ratio. The geometrical dimension of all compression specimens in groups a, b and c is presented in Table 2.

#### Oven-dry density analysis and the moisture contents (MC) determination

According to the international standards ISO 22157-2019 [20] and ISO 23478-2022 [19], the best way to obtain the air-dry density is through using a conventional oven-dry method as follows:

1. The dimensions were measured for the chosen 15 samples at a precision of at least 0.1 mm to estimate their initial volume  $V_0$  and weighing were carried out to obtain the original mass  $m_0$ .
2. Then, the specimens were placed in the oven at a temperature of 103 °C for 24 h to dry. After the 24 h long drying, the process continued until the constant oven-dry mass were reached, that is, until hourly mass measurement ( $m_i$ ) showed smaller deviation than 0.5% of the original specimen mass  $m_0$ . The final weighing was carried out immediately afterward. Hence, the mass  $m_{dry}$  of the oven-dry test specimens was determined to a precision of 0.5% of the original specimen mass  $m_i$ . The basic dry density  $\rho$  was obtained from the formula:

$$\rho = \frac{m_{dry}}{V_0}. \quad (1)$$

The MC of the 15 axial compression specimens was also calculated as

$$MC(\%) = \frac{m_0 - m_{dry}}{m_{dry}} \times 100. \quad (2)$$

#### Compression tests parallel-to-grain (group a), and perpendicular-to-grain (groups b and c)

In each test group, 16 specimens were tested. All tested samples were planned and prepared in compliance to the procedure outlined in the first international bamboo standard ISO 23478-2022 [19].

As shown in Table 2, the compression specimens in group a had dimensions 37 mm length (axis  $x$ ), 36 mm width (axis  $y$ ) and 74 mm height (axis  $z$ ). The effective gauge length was taken as the initial height  $h_0$  before commencing the test, see Fig. 3b. 16 compression specimens were conditioned and stored at a climate-room environment as prescribed in ISO 23478-2022 [19]; the temperature was set about  $20 \pm 2$  °C and a relative humidity was about  $65 \pm 5\%$  for 24 h.

All compression test samples were conducted using a universal material testing machine Zwick Z400, equipped with 479 kN capacity load head, see Fig. 3. Of the 16 cuboid specimens prepared for the test, 5 were equipped with strain gauges for accurate measurements of elastic moduli and Poisson's ratios. Each sample was placed into the compression area and fixed with two plates at the top and bottom faces of the sample. The crosshead displacement was treated as a compressive deformation controlled in parallel and perpendicular-to-grain directions. For the compression tests parallel-to-grain direction in group a, the specimens were compressed using a testing machine Zwick Z400, equipped with 479 kN capacity load head at a crosshead displacement rate of 1 mm/min up to fracture. By setting the upper limit of the applied load to 100 kN, the maximum compression displacement was measured to reach less than 16 mm. The specimens of group b and c were loaded at a crosshead displacement rate of 1 mm/min up to fracture. By setting the upper limit of the applied load for tangential and radial directions was set to 40 kN, the maximum compression displacement reached less than 13 and 9 mm for tangential (group b) and radial (group c) direction, respectively. All tested specimens were completed within 300 s as outlined in ISO 23478-2022 [19]. The strain gauge sensors were supplied by a Hungarian company MikroT corp., its nominal resistance is  $350 \Omega \pm 0.3\%$ , its gauge length is 3 mm, and its grid width is 3 mm. Figure 3b shows the layout of the strain gauges on the faces of specimens from group a. The elastic modulus in compression tests parallel-to-grain was suggested by ISO 23478-2022 to be calculated as

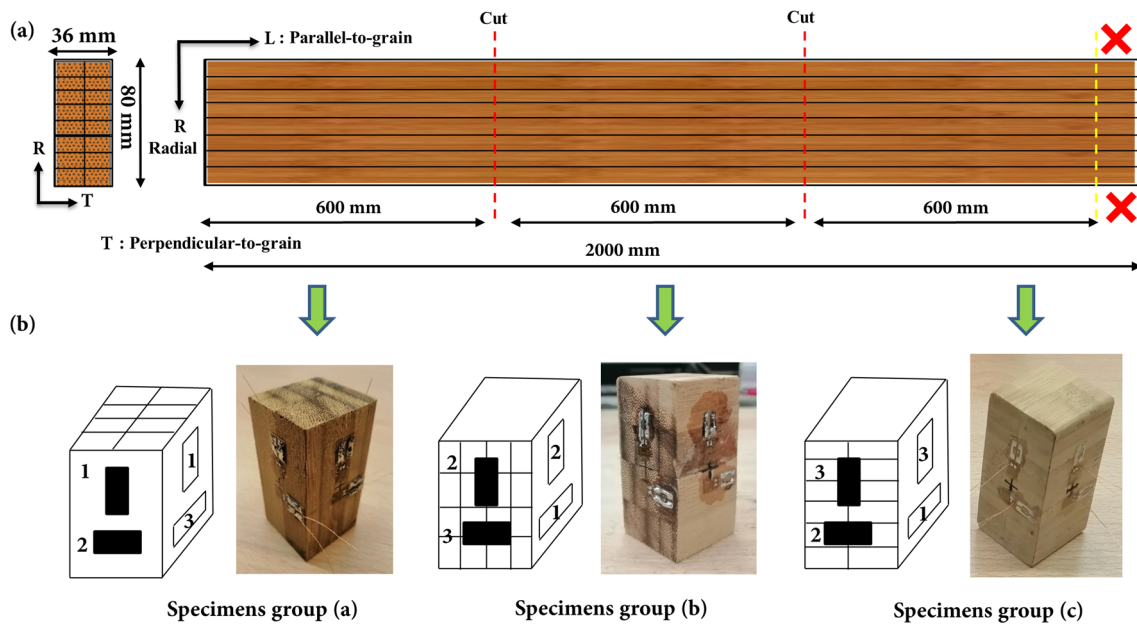


**Fig. 2** Steps of preparing compression specimens with (a) N-finity beam cut, (b) 48 compression specimens indicating the locations of the strain gauges by black rectangles; the layouts of strain gauges and corresponding images of compression specimens are shown in group (a), group (b) and group (c), respectively.

**Table 2** Geometrical dimension of all compression specimens (unit: mm)

Compression specimens	Length <i>l</i>	Width <i>b</i>	Height or depth <i>h<sub>0</sub></i>
Group (a)	38	36	74
Group (b)	37	36	74
Group (c)	37	36	73

$$E_{c,0} = \frac{l_1(F_{40} - F_{10})}{b \cdot h(\Delta_{40} - \Delta_{10})}, \tag{3}$$

where  $l_1$  is the gauge length of the sample,  $F_{40}$  and  $F_{10}$  are the applied load at 40% and 10% of  $F_{max}$ , respectively,  $\Delta_{40}$  is the displacement corresponding to load  $F_{40}$ ,  $\Delta_{10}$  is the displacement corresponding to load  $F_{10}$ ,  $b$  and  $h$  are cross-sectional dimensions of the specimen. The compressive strength parallel-to-grain was calculated as

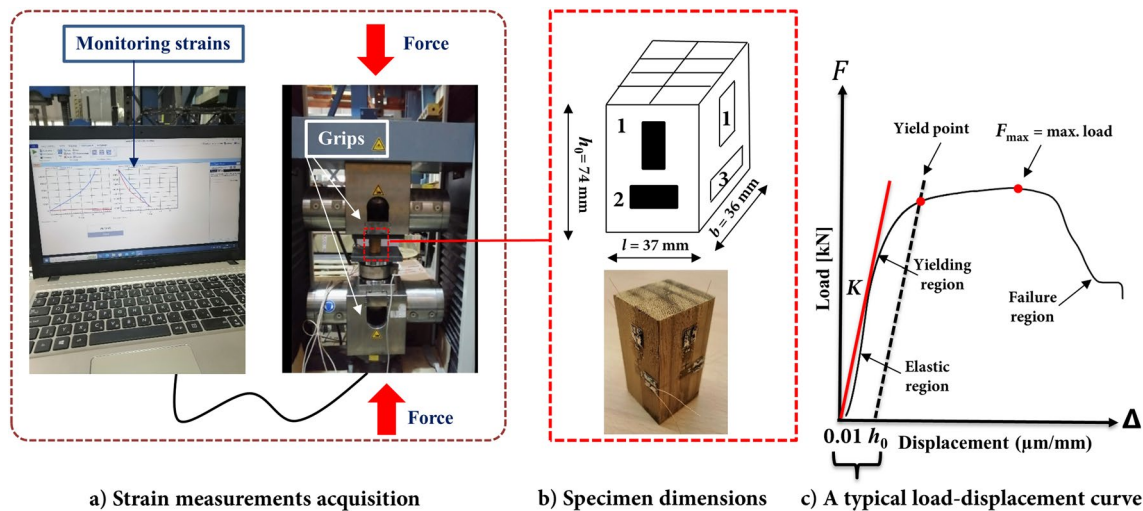


**Fig. 3** Schematic overview of the strain measurements and the compression test specimen. **a** Strain measurement acquisition, **b** compression test specimen, and **(c)** a typical representation of the load–displacement curve of a compression specimen

$$f_{c,0} = \frac{F_{\max}}{b \cdot h}, \tag{4}$$

where  $F_{\max}$  is the ultimate load,

The elastic modulus in compression tests perpendicular-to-grain (tangential and radial) was suggested by ISO 23478-2022 to be calculated as

$$E_{c,90} = \frac{h_0(F_{40} - F_{10})}{b \cdot l(\Delta_{40} - \Delta_{10})}, \tag{5}$$

where  $h_0$  is the original sample height,  $l$  is the length of the specimen.  $F_{40}$  and  $F_{10}$  are the applied load at 40% and 10% of  $F_{c,90,\max}$ , respectively. The compressive strength perpendicular-to-grain (tangential and radial) was calculated as

$$f_{c,90} = \frac{F_{c,90,\max}}{b \cdot l}. \tag{6}$$

Figure 3c shows the typical load–displacement curve of test specimen to determine the compressive strengths. The yield point in Fig. 3c is  $F_{c,90,\max}$  which can be defined as the maximum compressive load perpendicular-to-grain (tangential and radial).

## Results and discussion

### Oven-dry density measurements

The results of the physical determination of the oven-dry density and moisture content for axial compression specimens parallel and perpendicular-to-grain directions are summarised in Table 3. The mean value of MC of the samples was measured to be ~ 7.2% in average, and an oven-dry density of 625 kg/m<sup>3</sup>.

### Compressive strength measurements of N-finity bamboo samples

This section presents the results of the measured compressive strengths both parallel and perpendicular-to-grain directions. The measured values, using Eqs. (4) and (6), are summarised in Table 4. As can be seen, the ultimate compressive strength parallel-to-grain direction shows the highest value of about 68 MPa in average as compared to perpendicular-to-grain tangential and radial directions with 15 MPa and 13 MPa, respectively.

In Table 4,  $\sigma_{11}$  is the compressive strength parallel-to-grain,  $\sigma_{22}$  is the compressive strength perpendicular-to-grain in the tangential direction and  $\sigma_{33}$  is the compressive strength perpendicular-to-grain in the radial direction. The coefficient of variation (COV)

**Table 3** Measurement of the oven-dry density and moisture content after uniaxial compression testing the specimens

Sample no.	Length (mm)	Width (mm)	Height/ depth (mm)	Volume (mm <sup>3</sup> ) × 1000	Mass (g)			MC%	Density (kg/cm <sup>3</sup> )
					0 h	3 h	2 h		
					$m_0$	$m_{dry}$	$m_i$		
$l$	$b$	$h_0$	$V_0$				$\rho$		
2a	38.89	36.56	73.64	1047.02	69.8	64.5	64.5	7.59	616.03
4a	38.64	36.63	73.47	1039.88	68.9	64.1	64.0	6.96	616.41
6a	38.33	36.56	73.96	1036.43	71.5	66.4	66.4	7.13	640.65
8a	38.91	36.58	72.77	1035.75	65.8	61.1	61.1	7.14	589.91
12a	37.27	36.58	74.30	1012.96	67.0	62.4	62.4	6.86	616.01
4b	37.56	36.55	74.42	1021.65	72.2	66.6	66.6	7.75	651.88
7b	37.29	36.52	74.29	1011.70	70.5	65.5	65.5	7.09	647.42
9b	37.29	36.52	74.29	1011.70	71.5	66.4	66.4	7.13	656.31
15b	37.43	36.59	74.16	1015.66	70.7	65.6	65.6	7.21	645.88
16b	37.39	36.45	73.00	994.89	71.5	66.5	66.5	7.01	668.41
2c	36.95	36.79	73.05	993.03	65.2	60.1	60.1	7.82	605.21
9c	37.05	37.87	73.11	1025.79	68.2	63.3	63.3	7.18	617.08
10c	37.08	37.02	72.28	992.18	65.5	60.8	60.8	7.17	612.78
11c	37.12	36.74	72.86	993.65	64.2	59.7	59.7	7.01	600.81
13c	37.26	35.80	72.87	972.01	62.4	58.0	58.0	7.05	596.70
Mean								7.20	625.43
STD								0.27	23.41

Letters in the sample no. indicate the sample group a, b or c

**Table 4** Compressive strength measurements of N-finity bamboo for all samples

Strength	Sample	Dimension: mm		Height $h_0$	Area (A) (mm <sup>2</sup> )	Max. load N	Strength MPa	Mean MPa	STD	COV %
		b	l							
$\sigma_{11}$	1	36.51	37.53	74.26	1406.73	97000	68.95	68.60	1.09	1.58
	2	36.56	38.89	73.64	1421.81	97762	68.75			
	3	36.56	38.74	73.86	1416.33	95510	67.43			
	4	36.63	38.64	73.47	1415.38	99425	70.24			
	5	36.55	38.20	73.47	1396.21	95219	68.19			
	6	36.56	38.33	73.96	1401.34	99293	70.85			
	7	36.56	38.18	73.36	1395.81	96835	69.37			
	8	36.58	38.91	72.77	1423.32	96571	67.84			
	9	36.65	37.43	73.85	1371.81	95142	69.35			
	10	36.52	38.22	74.02	1395.79	94000	67.34			
	11	36.57	38.09	73.99	1382.59	95328	68.94			
	12	36.58	37.27	74.30	1363.33	92921	68.15			
	13	36.48	37.90	74.52	1382.59	95328	68.94			
	14	36.51	37.67	73.71	1375.33	95208	69.22			
	15	36.68	38.07	73.78	1396.40	92935	66.55			
	16	36.57	37.53	73.76	1372.47	92516	67.40			
$\sigma_{22}$	1	36.6	37.45	74.34	1370.67	22500	16.41	15.41	0.50	3.20
	2	36.57	37.2	74.71	1360.40	20133	14.80			
	3	36.57	36.62	74.59	1339.19	21914	16.36			
	4	36.55	37.56	74.42	1372.82	22136	16.12			
	5	36.67	37.46	74.41	1373.65	21222	15.45			
	6	36.48	37.38	74.52	1363.62	20152	14.78			
	7	36.52	37.29	74.29	1361.83	20032	15.44			
	8	36.48	37.31	74.32	1361.07	20652	15.17			
	9	36.52	37.29	74.29	1361.83	20465	15.03			
	10	36.54	37.32	74.23	1373.60	20778	15.13			
	11	36.54	37.32	74.23	1363.67	21163	15.52			
	12	36.48	37.35	74.11	1362.53	20511	15.05			
	13	36.54	37.32	74.23	1363.67	20637	15.13			
	14	36.53	37.25	74.10	1360.74	21000	15.43			
	15	36.59	37.43	74.16	1369.56	20548	15.05			
	16	36.45	37.39	73	1362.86	21423	15.72			
$\sigma_{33}$	1	36	37.48	73.14	1349.28	25343	18.78	13.16	4.43	33.68
	2	36.79	36.95	73.05	1359.39	22784	16.76			
	3	35.27	37.44	73.03	1320.51	22024	16.67			
	4	36.43	37.66	73.03	1371.95	22763	16.59			
	5	35.81	37.48	73.14	1342.15	23561	17.55			
	6	36.68	37.65	73	1381	6422	4.65			
	7	36.9	38.38	73.23	1416.22	18725	13.22			
	8	36.68	37.69	72.84	1382.47	13952	10.10			
	9	37.87	37.05	73.11	1403.08	25523	18.19			
	10	37.02	37.08	72.28	1372.70	14652	10.67			
	11	36.74	37.12	72.86	1363.80	17963	13.17			
	12	36.45	37.46	73	1365.42	11943	8.75			
	13	35.80	37.26	72.87	1334	10668	7.99			
	14	36.71	37.33	72.87	1370.38	8532	6.22			
	15	37.27	37.04	73.18	1380.48	24133	17.48			
	16	36.18	37.35	72.84	1351.32	18674	13.82			



is the ratio of the standard deviation (STD) to the mean of  $n = 16$  samples at each tested group. From the measured values, it can be found that the ratio of the maximum compressive load of parallel-to-grain direction is 4.45 higher than that of perpendicular-to-grain tangential direction and is 5.21 higher than that in the perpendicular-to-grain radial direction. These observed values are consistent with previous experimental studies using testing methods BS 373, GB/T1931-2009, GB/T1933-2009, GB/T 50329-2012, JG/T 199-2007, and BS EN 408 as listed in Table 1.

The load–displacement relationship curves of the specimens parallel and perpendicular-to-grain directions are shown in Fig. 4. From the graphs, one can see clearly that all specimens under compression show three distinct regions. The first one is a linear elastic behaviour up to the yield point marked as  $F_{c,90,max}$  followed by a nonlinear behaviour with plastic deformation region to reach a peak point identifies as a maximum applied load  $F_{max}$ , and finally the descending and rupture region can be identified. This supports the elastic–plastic compression model of LBL proposed

previously [10, 21]. The maximum compression displacement reached less than 16 mm for parallel-to-grain direction, whereas it was about 19 and 10 mm for perpendicular-to-grain tangential and radial directions, respectively.

#### Stress–strain relationship curves in compression using strain gauges

The compressive stress–strain relationship curves of the five selected test specimens in each group equipped with strain gauges are depicted in Fig. 5 both parallel and perpendicular-to-grain. The graph Fig. 5a for group a, illustrates a clear elastic–plastic behaviour of N-finity Moso bamboo, however, the graphs seem to suggest linear behaviour in Fig. 5b, c, especially, for groups b and c. In case of parallel-to-grain load, the elastic behaviour was remarkably linear up to about 60% of the applied load followed by a flattened plastic plateau as the load increases monotonically. In case of the tangential load direction, one can see considerable hardening for some samples. It is worth noting that no clear rupture region was seen in all graphs, which can be explained by the absence of clear rupture in

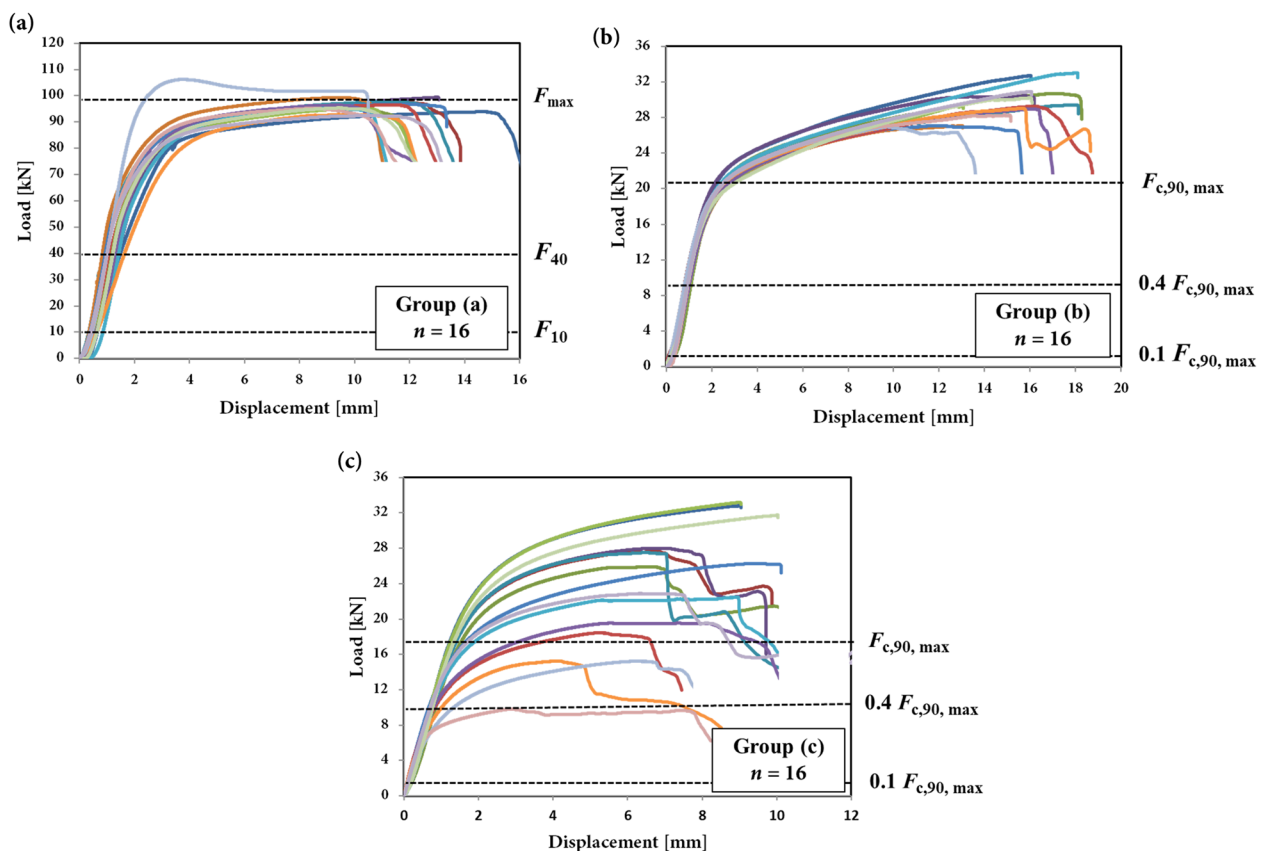


**Fig. 4** Load–displacement curves from the compressive experiments of N-finity Moso bamboo samples (a) parallel-to-grain, (b) perpendicular-to-grain tangential and (c) perpendicular-to-grain radial directions

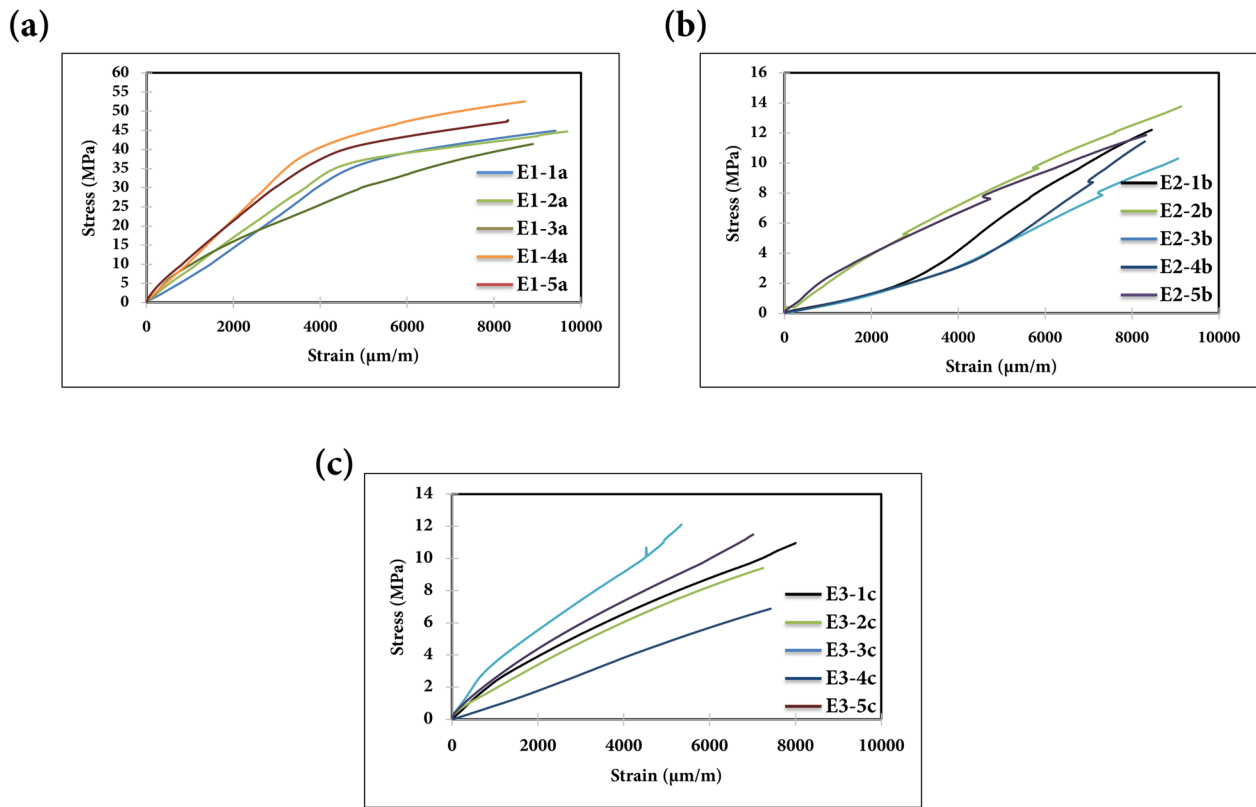


**Fig. 5** Stress–strain curves from the compressive experiments of N-finity Moso bamboo: (a) parallel-to-grain, axial (b) perpendicular-to-grain, tangential and (c) perpendicular-to-grain, radial directions

the strain values has to do with the fact that there was no rupture at the strain gauge positions and the maximum detected strain values of strain sensors were quite below of 10,000  $\mu\text{m/m}$ . From the measured stress–strain relationships, the elastic moduli in compression were calculated from the slope of the initial linear part, and the associated Poisson’s ratios were measured in three directions [14] as

$$\nu_{ii} = \frac{\Delta \varepsilon'}{\Delta \varepsilon} \quad (i = 1, 2, 3), \tag{7}$$

where  $\Delta \varepsilon'$  and  $\Delta \varepsilon$  are the lateral and axial strain increment, respectively.

**Elastic modulus and Poisson’s ratio in compression**

To evaluate the elastic properties of all test specimens, standard ISO 23478-2022 suggests computing

**Table 5** Evaluation of elastic moduli of N-finity bamboo measured using Eqs. (3) and (5)

Property	Samples	Without strain gauges			With strain gauges		
		$E_{11}$	$E_{22}$	$E_{33}$	$E_{11}$	$E_{22}$	$E_{33}$
Values ( $E$ ) in GPa	1	6.685	1.328	0.871	8.575	2.809	0.803
	2	8.626	1.604	1.245	8.178	0.773	0.995
	3	11.373	1.822	0.727	10.230	1.385	0.784
	4	7.895	1.802	0.783	10.001	0.855	0.576
	5	9.170	1.737	0.729	10.530	0.753	0.633
Mean		8.75	1.659	0.871	9.50	1.32	0.76
STD		1.55	0.18	0.22	0.94	0.78	0.15
COV %		17.75	10.97	22.29	9.92	59.4	20

the elastic moduli using Eqs. (3) and (5). In Table 5, the values obtained this way are compared with those obtained from measurements by strain gauges. It is found that the majority of values (except  $E_{11}$ ) obtained from specimens equipped with strain gauges show higher variability. Indeed, given the asymmetry of the deformations indicated in stress–strain relationship curves in compression using strain gauges, a significant part of the deformations occurs outside the position of the strain gauges, leading to false values not characteristics of the whole length of the sample. Thus, we find it more reliable to obtain the elastic moduli using Eqs. (3) and (5) from standard ISO 23478-2022 rather than measuring the strains directly by strain gauges.

Then, to compute the shear moduli in three directions, the formula was used, see [22] and [23] cited in [8]:

$$G_{12} = \frac{\sqrt{E_{11}E_{22}}}{2(1 + \sqrt{\nu_{21}\nu_{12}})}, G_{13} = \frac{\sqrt{E_{33}E_{11}}}{2(1 + \sqrt{\nu_{31}\nu_{13}})}, G_{23} = \frac{\sqrt{E_{22}E_{33}}}{2(1 + \sqrt{\nu_{32}\nu_{23}})}, \tag{8}$$

where  $G_{ij}$  and  $E_{ii}$  are the shear moduli and elastic moduli in three directions, respectively,  $\nu_{ii}$  are the Poisson’s ratios in three directions. Even though, it is highly preferable, that the shear moduli must be determined from some shear tests including the shear test of composite laminates (Iosipescu), asymmetric four-point bending, and off-axis loading tests. Table 6 summarises all measured elastic properties and calculated shear moduli of the five test specimens equipped with strain gauges in three directions (longitudinal, tangential, radial) of N-finity Moso bamboo. It is observed that group a, compression parallel-to-grain shows significantly higher elastic modulus than the other two directions by the ratio of

5.23 for tangential (group b) and of 6.55 for radial direction (group c). These observed trends are consistent with those found previously for LBL columns [8, 11, 14]. The mean shear moduli were obtained from Eq. (8) using the mean values of the elastic moduli and Poisson’s ratios.

**Typical failure mode mechanisms of N-finity samples in compression**

The ultimate load capacity of N-finity, which is composed of glued bamboo strips, depends on the failure mode and the amount of fibres present in the specific failure location. Here, the typical failure of bamboo specimens in all three investigated groups a, b and c were examined. The three main modes of failure are depicted in Fig. 6 and Table 6. These failure mechanisms are as follows: Mode 1 is a combined mechanism entailing buckling of fibres (tearing) within the depth of the specimen and separa-

tion of fibres at the bottom corner of specimen and at the mid height. Mode 2 is a local buckling and shear failure occurring diagonally at the bottom corner of the specimen. Mode 3 constitutes a propagation of cracks inside the individual glued bamboo strips. The cracks occurred at the bamboo strips themselves in each tested specimen of group b, whereas cracks were inclined at one particular corner of each tested specimen of group c. It was noted that no adhesive failure or cracks were observed at the bamboo strips-glue interface, hence both fibres and adhesive glue were considered intact until the end of the compression tests.

**Table 6** Measured elastic properties of N-finity bamboo (layout is adopted from [14])

Groups	Constants (E and G) in GPa	Specimen no.					Mean	STD	COV %
		1	2	3	4	5			
Group (a)	$E_{11}$	6.685	8.626	11.373	7.895	9.170	8.75	1.55	17.75
	$\nu_{12}$	0.181	0.185	0.221	0.211	0.373	0.23	0.07	30.33
	$\nu_{13}$	0.257	0.429	0.221	0.315	0.362	0.32	0.07	23.36
Group (b)	$E_{22}$	1.979	2.203	2.185	2.279	2.305	2.19	0.11	5.24
	$\nu_{21}$	0.051	0.061	0.047	0.035	0.039	0.05	0.01	19.65
	$\nu_{23}$	0.654	0.107	0.871	0.594	0.409	0.53	0.25	48.70
Group (c)	$E_{33}$	1.107	1.524	0.999	1.050	0.888	1.11	0.21	19.53
	$\nu_{31}$	0.048	0.045	0.052	0.095	0.031	0.05	0.02	39.83
	$\nu_{32}$	0.466	0.842	0.541	0.51	0.425	0.55	0.15	26.56
Calculated	$G_{12}$						1.97	–	–
	$G_{13}$						1.38	–	–
	$G_{23}$						0.51	–	–

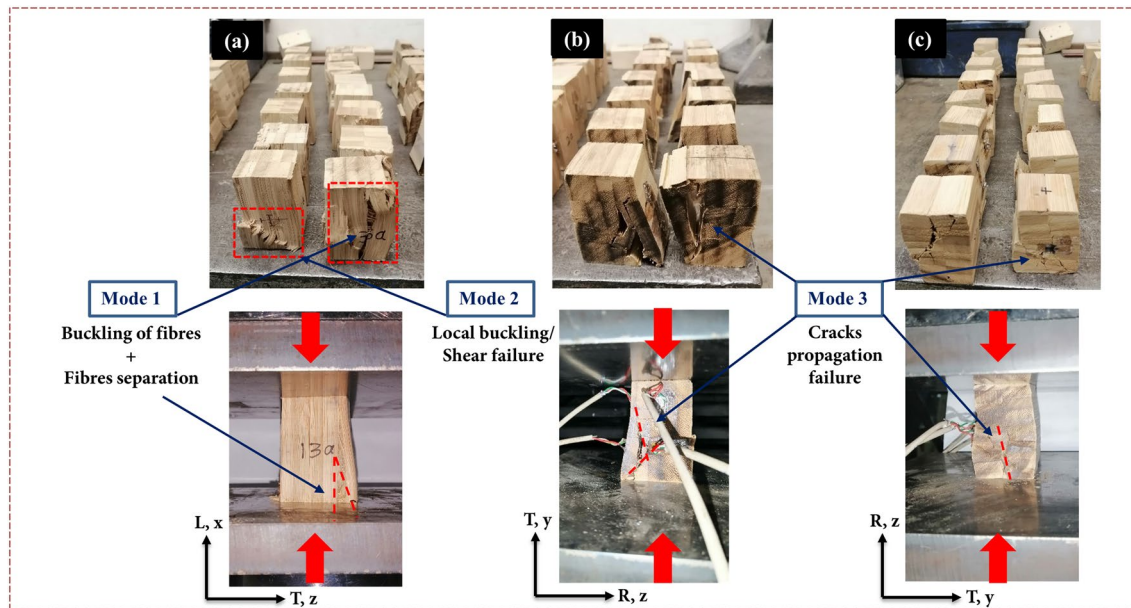


**Fig. 6** Failure modes of N-finity Moso bamboo samples in compression as observed in the experiments (see text for description). Letters in black background refer to the test groups a, b and c

**Table 7** Failure modes of the N-finity Moso bamboo

Testing group	Testing direction	Specimen no.	Failure modes		
			1	2	3
Group a	Parallel-to-grain (axial)	16	16	16	0
Group b	Perpendicular-to-grain (tangential)	16	0	0	16
Group c	Perpendicular-to-grain (radial)	16	0	0	16

Table 7 illustrates the failure modes of the 48 investigated compression specimens parallel and perpendicular-to-grain directions. It can be concluded that all compression samples parallel-to-grain direction exhibited a mixed mode failure, mode 1 and 2, whereas specimens of group b and c, perpendicular-to-grain directions exhibited failure mode 3, longitudinal splitting with crack propagation rupture. These observations were consistent with those reported by [1, 8, 10, 16, 24] for laminated bamboo.

**Hill’s failure criterion and mechanical properties of N-finity Moso bamboo**

From the results of the previous section, it is evident that N-finity Moso bamboo has directionally dependent properties with higher compressive strength and elastic properties parallel-to-grain direction and lower values at

transversal directions. In addition, there is some difference between the elastic properties in the two transversal directions. This physical anisotropy is caused by the anisotropic material properties which were observed by the authors previously while developing an anatomy-based numerical model of bamboo microstructure [25]. Hence, in this section, the failure criterion of LBL is investigated by estimating Hill’s yield failure ratios  $R_{ij}$  in the parallel and perpendicular-to-grain directions. This is important for the development of an accurate computational model and analysis of N-finity bamboo with any finite element modelling package such as ANSYS. As N-finity bamboo shows anisotropy in strength and the associated stiffness properties, the anisotropic Hill’s plasticity principle can be applied to characterise its failure criterion. According to Tang et al. [14] and Hong et al. [8], Hill’s failure criterion evaluates the strength of EBPs such as a laminated bamboo N-finity as:

$$f(\sigma_{ij}) = \sqrt{F(\sigma_{22} - \sigma_{33})^2 + G(\sigma_{33} - \sigma_{11})^2 + H(\sigma_{11} - \sigma_{22})^2 + 2L\sigma_{23}^2 + 2M\sigma_{31}^2 + 2N\sigma_{12}^2} < \sigma^0, \tag{9}$$

where  $\sigma^0$  is the reference yield stress obtained from a uniaxial compression test in the parallel-to-grain direction,  $\sigma_{11}$ ,  $\sigma_{22}$ , and  $\sigma_{33}$  are the normal stresses as presented in the previous Section,  $\sigma_{12}$ ,  $\sigma_{23}$ , and  $\sigma_{31}$  are the in-plane shear stress in plane 1–2, the out-of-plane shear stress in plane 2–3, and the out-of-plane shear stress in plane 1–3, respectively. F, G, and H are Hill’s yield surface coefficients estimated from three compression tests, whereas L, M, and N are surface coefficients obtained from shear tests. For a complete elaboration on the set of equations to calculate these coefficients and Hill’s yield failure ratios  $R_{ii}$  with respects to the axes of orthotropy, see Tang et al. [14] and Hong et al. [8]. The failure ratios  $R_{ii}$  can be calculated as:

$$R_{11} = \frac{f_{11}}{\sigma^0}, R_{22} = \frac{f_{22}}{\sigma^0}, R_{33} = \frac{f_{33}}{\sigma^0}, R_{12} = \frac{f_{12}}{\tau^0}, R_{13} = \frac{f_{13}}{\tau^0}, R_{23} = \frac{f_{23}}{\tau^0}, \tau^0 = \frac{\sigma^0}{\sqrt{3}}, \tag{10}$$

where  $f_{11}$ ,  $f_{22}$ ,  $f_{33}$  are the strength values of N-finity bamboo corresponding to the measured stresses parallel and perpendicular-to-grain compression tests in the three material directions 1, 2, and 3, respectively;  $f_{12}$ ,  $f_{23}$ , and  $f_{13}$  are the strength corresponding to the measured stresses obtained from shear tests in three planes: the in-plane strength in plane 1–2, the out-of-plane strength in plane 2–3, and the out-of-plane strength in plane 1–3, respectively. Also,  $\sigma^0$  is the stress obtained from our uniaxial compression test parallel-to-grain direction, and it was taken to be equal to the compression strength  $f_{11}$ , see Tang et al. [14] and Hong et al. [8]. The stiffness properties of N-finity Moso bamboo are summarised in Table 8. The orthotropic yield strengths and the calculated Hill’s yield ratios are based on the measured compressive strengths at three material directions 1, 2, and 3, whereas the shear strengths values were computed for simplicity and thus, their values were obtained from Eq. (11) at three planes of orthotropy (1–2), (2–3) and (1–3), respectively, see [26] cited in [27]

$$\gamma_{12} = \frac{f_{11}}{1.98E_{11}} \sqrt{\frac{E_{11}}{G_{12}}}, \gamma_{13} = \frac{f_{33}}{1.98E_{33}} \sqrt{\frac{E_{33}}{G_{13}}}, \gamma_{23} = \frac{f_{22}}{1.98E_{22}} \sqrt{\frac{E_{22}}{G_{23}}}, \tag{11}$$

where  $\gamma_{12}$ ,  $\gamma_{13}$ , and  $\gamma_{23}$  are the shear strain in planes 1–2, 1–3, and 2–3, respectively.

### Conclusions and future work

This study evaluates the mechanical properties of N-finity Moso bamboo under uniaxial compression utilising the recently published ISO 23478-2022 standard for testing structural specimens of EPBs including LBL. The test programme was conducted on 48 small clear specimens at three orthogonal directions. The experimental results

include overall mechanical properties like elastic moduli in compression, Poisson’s ratios, shear moduli as well as the strength properties in compression parallel and perpendicular-to-grain directions. It can be found the expected anisotropy of the mechanical properties, with higher values of the mechanical properties in the parallel-to-grain direction. The oven-dry density and moisture content of the specimens were also determined. As the final point of the compression tests, the failure modes of the N-finity samples were also presented and further discussed. Finally, Hill’s yield surface coefficients were estimated, using the anisotropic Hill’s plasticity principle to support later numerical modelling of bamboo taking into account its anisotropy.

The following conclusions can be drawn from the present study:

- The measured compressive strength utilising the recently published ISO 23478-2022 standard shows the highest value of about 68 MPa in average in the

**Table 8** Summary of mechanical properties of N-finity Moso bamboo with moisture content 7.2% on average

Engineering constants	Elastic modulus (GPa)			Poisson’s ratio			Shear modulus (GPa)		
	$E_{11}$	$E_{22}$	$E_{33}$	$\nu_{12}$	$\nu_{13}$	$\nu_{23}$	$G_{12}$	$G_{13}$	$G_{23}$
	8.75	2.19	1.11	0.24	0.35	0.52	1.97 <sup>a</sup>	1.38 <sup>a</sup>	0.51 <sup>a</sup>
Calculated Hill’s yield ratios	$R_{11}$	$R_{22}$	$R_{33}$	$R_{12}$	$R_{13}$	$R_{23}$			
	1	0.22	0.19	0.40	0.17	0.11			
Strength (MPa)	Compression strengths (yield)			Shear strengths (yield)					
	$f_{11}$	$f_{22}$	$f_{33}$	$f_{12}$	$f_{13}$	$f_{23}$			
	68.6	15.41	13.16	16.03 <sup>b</sup>	6.59 <sup>b</sup>	4.43 <sup>b</sup>			

Sources: a = calculated from Eq. (8), b = calculated from Eq. (11)

parallel-to-grain direction. The corresponding values perpendicular-to-grain in the tangential and radial directions were 15 and 13 MPa, respectively. This indicates that the ratio of the maximum compressive load in the parallel-to-grain direction to that in the tangential direction is 4.45, and to that in the radial direction is 5.21.

- The elastic modulus in compression follows the same trend: parallel-to-grain  $E_{11}$  is 8.75 GPa, in the tangential direction  $E_{22}$  is 2.19 GPa, and in the radial direction  $E_{33}$  is 1.11 GPa. This implies that compression parallel-to-grain shows significantly higher elastic modulus than that in the other two orthogonal directions by the ratio of 5.23 for tangential and of 6.55 for radial direction.
- The assessment of failure mechanisms concluded that all compression samples parallel-to-grain direction exhibited a combined mode failure, modes 1 and 2, whereas the perpendicular-to-grain directions exhibited failure mode 3, longitudinal splitting with crack propagation rupture, in all investigated cases.
- The bamboo samples had a moisture content of 7.2% and an oven-dry density of 625 kg/m<sup>3</sup> as captured according to the national bamboo standards ISO 22157-2019 and ISO 23478-2022.
- Further investigation is required to confirm the applicability of the anisotropic Hill's plasticity principle to estimate Hill's yield surface coefficients. This result is important to achieve an accurate numerical modeling of the anisotropy of the mechanical properties of LBL.

As a possible next step, the authors plan to conduct a physical experimental programme on short steel-bamboo columns subjected to pure compression. The motivation is that for building lightweight structural applications applying bamboo, it is important to assess the mechanical performance and local buckling mechanism of LBL.

#### Abbreviations

LBL	Laminated bamboo lumber
EBPs	Engineered bamboo products
$E_{c,0}$	Modulus of elasticity in compression tests parallel-to-grain
$l_1$	The gauge length of the sample
$F_{max}$	The ultimate load
$F_{40}$	The applied load at 40% of $F_{max}$
$F_{10}$	The applied load at 10% of $F_{max}$
$\Delta_{40}$	The displacement corresponding to load $F_{40}$
$\Delta_{10}$	The displacement corresponding to load $F_{10}$
$b$ and $h$	Cross-sectional dimensions of the specimen
$f_{c,0}$	The compressive strength parallel-to-grain
$E_{c,90}$	The modulus of elasticity in compression tests perpendicular-to-grain
$h_0$	The original sample height
$l$	Length of the specimen

$f_{c,90}$	The compressive strength perpendicular-to-grain
$MC$	Moisture content
$m_1$	Hourly mass measurement
$m_0$	Original specimen mass
$m_{dry}$	Oven-dry test specimens
$\rho$	The basic dry density
$V_0$	The initial sample volume
STD	Standard of deviation
COV	Coefficient of variation
$\sigma_{11}$	The ultimate compressive strength parallel-to-grain direction
$\sigma_{22}$	The ultimate compressive strength perpendicular-to-grain tangential
$\sigma_{33}$	The ultimate compressive strength perpendicular-to-grain radial
$\Delta \epsilon_l$	The lateral strain increment
$\Delta \epsilon$	The axial strain increment
$G_{ij}$	Shear moduli in three directions
$E_{ij}$	Elastic moduli in three directions
$\nu_{ij}$	Poisson's ratios in three directions
$\sigma^0$	The reference yield stress
$F, G, H, L, M, \text{ and } N$	Hill's yield surface coefficients
$R_{ij}$	Hill's yield failure ratios
$f_{11}, f_{22}, f_{33}$	Strengths corresponding to compression tests in the three material directions 1, 2, and 3, respectively
$f_{12}, f_{23}, \text{ and } f_{13}$	Strengths corresponding to shear tests in three planes: the in-plane strength in plane 1–2, the out-of-plane strength in plane 2–3, and the out-of-plane strength in plane 1–3, respectively
$\gamma_{12}, \gamma_{13}, \text{ and } \gamma_{23}$	Shear strain in planes 1–2, 1–3, and 2–3, respectively

#### Acknowledgements

Not applicable.

#### Author contributions

LSA: Conceptualization, Methodology, Writing—original draft, Physical testing, Formal analysis, Validation, Resources. MK: Physical testing, Writing—review and editing. GK: Writing—review and editing, Supervision, Funding acquisition.

#### Funding

This work was supported by the Hungarian NKFIH under Grant No. K-128584, and by the NRD Fund of Hungary under Grant TKP2021-NVA-02. L S A-R was supported by the Stipendium Hungaricum scholarship scheme.

#### Availability of data and materials

All data generated or analysed during this study are included in this published article are available in figshare repository, which can be accessed from this link, <https://figshare.com/s/88840b57648a804cb91f>.

#### Declarations

#### Competing interests

The authors declare that they have no competing financial interests or personal relationships that could have appeared to influence the work reported in this paper.

Received: 24 August 2023 Accepted: 8 December 2023

Published online: 02 January 2024

#### References

1. Sharma B, Bauer H, Schickhofer G, Ramage MH (2017) Mechanical characterisation of structural laminated bamboo. *Proc Inst Civ Eng Struct Build* 170:250–264. <https://doi.org/10.1680/jstbu.16.00061>
2. Nugroho N, Ando N (2001) Development of structural composite products made from bamboo II: fundamental properties of laminated

- bamboo lumber. *J Wood Sci* 47:237–242. <https://doi.org/10.1007/BF01171228>
3. Ohuchi T, Nakahara M, Murase Y (2006) Cross-sectional cutting of bamboo with a pair of shearing blades for bamboo cube production. *J Wood Sci* 52:274–278. <https://doi.org/10.1007/s10086-005-0749-0>
  4. Li H, Wu G, Zhang Q, Su J-W (2016) Mechanical evaluation for laminated bamboo lumber along two eccentric compression directions. *J Wood Sci* 62:503–517. <https://doi.org/10.1007/s10086-016-1584-1>
  5. Zheng Y, Yi B, Tong Y, Peng Z (2020) Influence of assemble patterns on bonding strength of glued bamboo. *J Wood Sci* 66:60. <https://doi.org/10.1186/s10086-020-01907-x>
  6. Guan X, Yin H, Lin C, Zhan W (2022) Effect of layups on the mechanical properties of overlaid laminated bamboo lumber made of radial bamboo slices. *J Wood Sci* 68:1–7. <https://doi.org/10.1186/s10086-022-02047-0>
  7. Hong CK, Li HT, Xiong ZH, Lorenzo R, Corbi I, Corbi O, Wei DD, Yuan CG, Yang D, Zhang HZ (2020) Review of connections for engineered bamboo structures. *J Build Eng* 30:101324. <https://doi.org/10.1016/j.jobe.2020.101324>
  8. Hong CK, Li HT, Xiong ZH, Lorenzo R, Li X, Wang Z (2021) Axial compressive behavior of laminated bamboo lumber columns with a chamfered section. *Structures* 33:678–692. <https://doi.org/10.1016/j.istruc.2021.04.083>
  9. Yeh M-C, Lin Y-L (2012) Finger joint performance of structural laminated bamboo member. *J Wood Sci* 58:120–127. <https://doi.org/10.1007/s10086-011-1233-7>
  10. Li HT, Zhang QS, Huang DS, Deeks AJ (2013) Compressive performance of laminated bamboo. *Compos Part B Eng* 54:319–328. <https://doi.org/10.1016/j.compositesb.2013.05.035>
  11. Li HT, Su JW, Zhang QS, Deeks AJ, Hui D (2015) Mechanical performance of laminated bamboo column under axial compression. *Compos Part B Eng* 79:374–382. <https://doi.org/10.1016/j.compositesb.2015.04.027>
  12. Sharma B, Gatóo A, Bock M, Ramage M (2015) Engineered bamboo for structural applications. *Constr Build Mater* 81:66–73. <https://doi.org/10.1016/j.conbuildmat.2015.01.077>
  13. Li HT, Wu G, Zhang QS, Deeks AJ, Su J (2018) Ultimate bending capacity evaluation of laminated bamboo lumber beams. *Constr Build Mater* 160:365–375. <https://doi.org/10.1016/j.conbuildmat.2017.11.058>
  14. Tang G, Yin LF, Li ZJ, Li Y, You L (2019) Structural behaviors of bolted connections using laminated bamboo and steel plates. *Structures* 20:324–339. <https://doi.org/10.1016/j.istruc.2019.04.001>
  15. Chen G, Yu Y, Li X, He B (2020) Mechanical behavior of laminated bamboo lumber for structural application: an experimental investigation. *Eur J Wood Wood Prod* 78:53–63. <https://doi.org/10.1007/s00107-019-01486-9>
  16. Zhang H, Li HT, Li YJ, Xiong ZH, Zhang N, Lorenzo R, Ashraf M (2021) Effect of nodes on mechanical properties and microstructure of laminated bamboo lumber units. *Constr Build Mater* 304:124427. <https://doi.org/10.1016/j.conbuildmat.2021.124427>
  17. Sharma B, Eley D, Emanuel O, Brentnall C (2021) Mechanical properties of laminated bamboo designed for curvature. *Constr Build Mater* 300:123937. <https://doi.org/10.1016/j.conbuildmat.2021.123937>
  18. Gao D, Chen B, Wang L, Tang C, Yuan P (2022) Comparative study on clear specimen strength and member strength of side-pressure laminated bamboo. *Adv Civ Eng* 2022:1–11. <https://doi.org/10.1155/2022/2546792>
  19. ISO 23478 (2022) ISO 23478-2022 Bamboo structures—engineered bamboo products—test methods for determination of physical and mechanical properties
  20. ISO 22157 (2019) Bamboo structures—determination of physical and mechanical properties of bamboo culms—test methods. Switzerland, Int Organ Stand
  21. Goonewardena J, Ashraf M, Reiner J, Kafle B, Subhani M (2022) Constitutive material model for the compressive behaviour of engineered bamboo. *Buildings* 12:1490. <https://doi.org/10.3390/buildings12091490>
  22. Saliklis EP, Falk RH (2000) Correlating off-axis tension tests to shear modulus of wood-based panels. *J Struct Eng* 126:621–625. [https://doi.org/10.1061/\(ASCE\)0733-9445\(2000\)126:5\(621\)](https://doi.org/10.1061/(ASCE)0733-9445(2000)126:5(621))
  23. Ramirez F, Correal JF, Yamin LE, Atoche JC, Piscal CM (2012) Dowel-bearing strength behavior of glued laminated guadua bamboo. *J Mater Civ Eng* 24:1378–1387. [https://doi.org/10.1061/\(ASCE\)MT.1943-5533.0000515](https://doi.org/10.1061/(ASCE)MT.1943-5533.0000515)
  24. Dauletbek A, Li HT, Lorenzo R (2022) A review of basic mechanical behavior of laminated bamboo lumber. *J Renew Mater* 10:273–300. <https://doi.org/10.32604/jrm.2022.017805>
  25. Al-Rukaibawi LS, Omairey SL, Károlyi G (2021) A numerical anatomy-based modelling of bamboo microstructure. *Constr Build Mater* 308:125036. <https://doi.org/10.1016/j.conbuildmat.2021.125036>
  26. Saliklis EP, Urbanik TJ, Tokyay B (2003) Bilinear modelling of cellulosic orthotropic nonlinear materials. *J Pulp Pap Sci* 29:407–411
  27. Hong J-P, Barrett JD, Lam F (2011) Three-dimensional finite element analysis of the Japanese traditional post-and-beam connection. *J Wood Sci* 57:119–125. <https://doi.org/10.1007/s10086-010-1151-0>

## Publisher's Note

Springer Nature remains neutral with regard to jurisdictional claims in published maps and institutional affiliations.

**Submit your manuscript to a SpringerOpen<sup>®</sup> journal and benefit from:**

- Convenient online submission
- Rigorous peer review
- Open access: articles freely available online
- High visibility within the field
- Retaining the copyright to your article

Submit your next manuscript at ► [springeropen.com](https://www.springeropen.com)